Dual-Emissive Nanohybrid for Ratiometric Luminescence and Lifetime Imaging of Intracellular Hydrogen Sulfide

Qi Yu,[†] Kenneth Yin Zhang,[†] Hua Liang,[†] Qiang Zhao,[*,†] Tianshe Yang,[†] Shujuan Liu,[†] Chuanqi Zhang,[†] Zhengjian Shi,[†] Wenjuan Xu,[†] and Wei Huang[*,†,‡]

[†]Key Laboratory for Organic Electronics and Information Displays & Institute of Advanced Materials, Jiangsu National Synergistic Innovation Center for Advanced Materials (SICAM), Nanjing University of Posts & Telecommunications (NUPT), Nanjing 210023, China

[‡]Key Laboratory of Flexible Electronics (KLOFE) & Institute of Advanced Materials (IAM), Jiangsu National Synergistic Innovation Center for Advanced Materials (SICAM), Nanjing Tech University (NanjingTech), 30 South Puzhu Road, Nanjing 211816, China

ⓢ Supporting Information

ABSTRACT: We design a nanohybrid for the detection of hydrogen sulfide (H_2S) based on mesoporous silica nanoparticles (MSNs). A phosphorescent iridium(III) complex and a specific H_2S-sensitive merocyanine derivative are embedded into the nanohybrid. It exhibits a unique dual emission that is ascribed to the iridium(III) complex and the merocyanine derivative, respectively. Upon addition of sodium hydrogen sulfide (NaHS), the emission from the merocyanine derivative is quenched, while the emission from the iridium(III) complex is almost unchanged, which enables the ratiometric detection of H_2S. Additionally, the nanohybrid has a long luminescence lifetime and displays a significant change in luminescence lifetime in response to H_2S. Intracellular detection of H_2S is performed via ratiometric imaging and photoluminescence lifetime imaging microscopy. Compared with the intensity-based method, the lifetime-based detection is independent of the probe concentration and can efficiently distinguish the signals of the probe from the autofluorescence in complex biological samples.

KEYWORDS: hydrogen sulfide, imaging, luminescence, nanoparticles, sensors
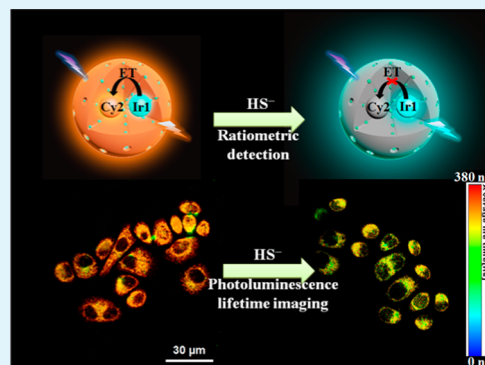
INTRODUCTION

Hydrogen sulfide (H_2S), with a smell compared to that of rotten eggs, is generally treated as a toxic gas and environment contaminant.[1,2] Hydrogen sulfide (H_2S) is a weak acid in aqueous solution ($pK_a = \sim 7.0$), equilibrating mainly with HS^-.[3] In biology, endogenous H_2S has gradually been discovered over the past decade in mammalian tissues. The synthesis process of H_2S has been demonstrated to be associated with several enzymes, such as cystathionine β-synthase (CBS), cystathionine γ-lyase (CSE), 3-mercaptopyruvate sulfurtransferase (3-MST) and cysteine aminotransferase (CAT).[3,4] Along with nitric oxide (NO) and carbon monoxide (CO), H_2S is qualified as the third endogenous gasotransmitter because of its significant roles in an array of intracellular signaling processes.[5,6] The intracellular concentration of mobile H_2S is tightly regulated. Failure of H_2S homeostasis has been linked to the pathogenesis of Alzheimer's disease,[7] Down's syndrome[8] and diabetic complications.[9] Hence, increasing attention has been drawn to sensitive and selective detection of H_2S in biological system.

Many fluorescent molecules, based on the nitro and azide reduction,[10−14] Michael addition reaction,[15,16] nucleophilic addition,[17−19] redox chemistry of the versatile selenium[20,21] and quencher (such as Cu^{2+}) removal,[22] have been reported to quantify H_2S. Most of these probes exhibit high sensitivity and selectivity in intracellular detection of H_2S via luminescence imaging techniques. These fluorescent probes, however, have limitations imposed by responses at a single detection window, which can be affected by the experimental conditions, such as the change of incident laser power and probe concentration. An alternative method is to design a ratiometric probe that can exhibit a change in the ratio of multiple emission bands in the presence of analyte. For example, He, Guo and co-workers reported a ratiometric fluorescent merocyanine-based probe which displays rapid and selective response to intracellular H_2S.[23]

In addition to intensity-based probes, lifetime-based probes have aroused great interest.[24−27] These probes provide the information on the analyte through obvious changes in emission lifetimes upon interaction with the analyte. The rapid development of photoluminescence lifetime imaging microscopy (PLIM) enables the lifetime-based detection of intracellular analytes. In PLIM imaging, luminescence lifetime is
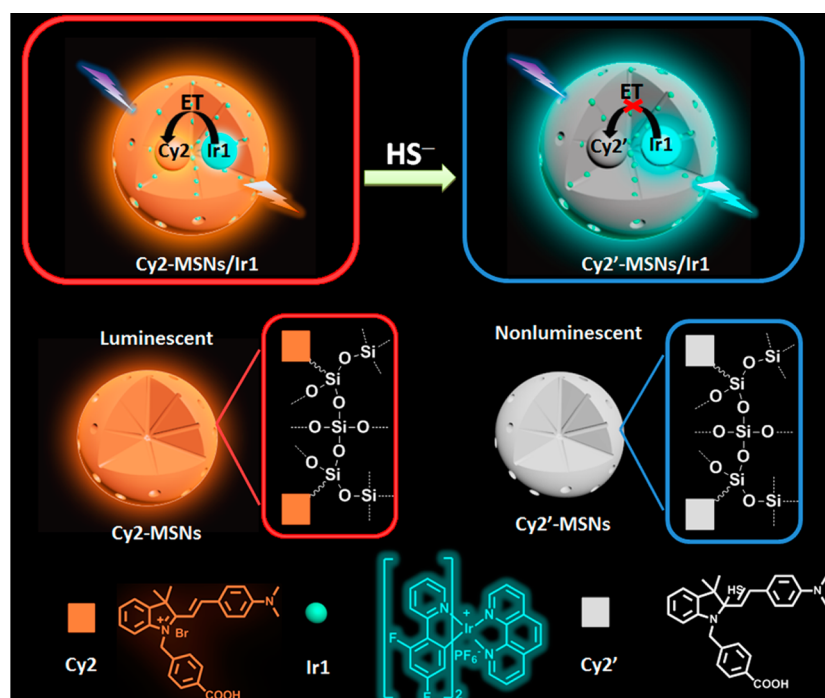
Figure 1. Design and architecture of the nanohybrid for the detection of H₂S.

measured at each spatially resolvable element of a microscope image,[28] and the lifetime obtained is independent of probe concentration and excitation laser intensity.[29] Additionally, when long-lived luminescent probes are employed for PLIM imaging, the signals from the probes can be distinguished from the autofluorescence,[30−35] which typically has a fluorescence lifetime ranging from the picosecond to nanosecond level. Phosphorescent transition-metal complexes (PTMCs) display triplet emission with lifetimes in the micro- or submicrosecond time scale due to spin−orbit coupling imparted by the heavy atom effect, allowing them to be applied for background-free sensing in complicated biosamples via PLIM imaging. Moreover, PTMCs exhibit other merits, such as tunable excitation and emission wavelengths, significant Stokes shifts (often >5000 cm^{-1}) and high photostability, rendering PTMCs as a promising class of probes for bioimaging.[36−43]

Herein, as illustrated in Figure 1, we designed a nanohybrid based on mesoporous silica nanoparticles (MSNs) which was embedded with an iridium(III) complex **Ir1** and a specific H₂S-responsive merocyanine derivative **Cy2**, designated as **Cy2-MSNs/Ir1**. We anticipated that **Cy2-MSNs/Ir1** had unique dual emission bands, and showed changes in luminescence profile from dominance of the emission from **Cy2** to the emission from **Ir1** upon addition of NaHS (commercially available H₂S donor), which facilitated the ratiometric detection. Additionally, efficient energy transfer from **Ir1** to **Cy2** was also expected to result in long emission lifetime of the nanohybrid. Luminescence lifetime-based detection of H₂S was possible for **Cy2-MSNs/Ir1**. Utilization of **Cy2-MSNs/Ir1** for the detection of intracellular H₂S was demonstrated via ratiometric luminescence and PLIM imaging.

■ EXPERIMENTAL SECTION

Chemical Reagents. All chemical reagents, unless otherwise specified, were purchased from Sigma-Aldrich Chemical Company. All solvents for reaction and photophysical investigation were used without further purification.

Characterization. Nuclear magnetic resonance (NMR) spectra were recorded on Bruker ACF400 (400 MHz) instrument. Mass spectra were obtained with matrix-assisted laser desorption ionization time-of-flight mass spectrometry (MALDI-TOF/TOF, Bruker autoflex, MS3). Transmission electron microscopy (TEM) was conducted on a JEOL JEM-2100 transmission electron microscope at an acceleration voltage of 150 kV. Average particle size was measured by dynamic light scattering (DLS) on Zetasizer Nanoseries (Nano ZS90). ζ-Potential was measured by Zeta-plus ζ-potential analyzer. Nitrogen adsorption−desorption measurements were carried out on a 3H-2000PS2 surface area analyzer at 77 K using the volumetric method, and samples were degassed at 150 °C for 4 h under vacuum overnight before measurements. Brunauer−Emmett−Teller (BET) specific surface areas were calculated by using adsorption data at P/P_0 = 0.05−0.25 (five points collected). Pore size distributions were estimated from adsorption branches of the isotherms by using the Barrett−Joyner−Halenda (BJH) method. Powder small-angle X-ray diffraction (XRD) measurements were carried out on a Bruker Smart APEX CCD diffractometer at 40 kV and 20 mA using Cu Kα radiation (λ = 1.54 Å). Photoluminescence (PL) spectra were measured on Edinburgh FL 920 instrument. Emission lifetimes of the nanohybrid and the iridium(III) complex **Ir1** were measured on Edinburgh FL 920 instrument with a laser (379 nm) as the excitation source. Emission lifetime of the merocyanine derivative was obtained on HAMAMAT-SU compact fluorescence lifetime spectrometer C11367 with a laser (470 nm) as the excitation source. UV−vis absorption spectra were recorded on a UV-1700 Shimadzu UV−vis spectrophotometer. Photographs of the solution samples were taken with a Cannon EOC 400D digital camera under a hand-held UV lamp.

Synthesis of Ir1. The iridium(III) complex **Ir1** was prepared according to a previous method.[44,45]

^{1}H NMR (400 MHz, d_6-DMSO): δ (ppm) 8.94 (dd, J = 1.6 Hz, 8 Hz, 2H), 8.41 (s, 2H), 8.30 (dt, J = 1.2 Hz, 5.2 Hz, 4H), 8.06 (dd, J = 5.2 Hz, 8.4 Hz, 2H), 7.97 (dt, J = 1.2 Hz, 7.6 Hz, 2H), 7.53 (d, J = 5.6 Hz, 2H), 7.07 (ddd, J = 1.2 Hz, 5.6 Hz, 7.2 Hz, 2H), 7.01 (ddd, J = 2.4 Hz, 9.6 Hz, 12.4 Hz, 2H), 5.72 (dd, J = 2.4 Hz, 8.4 Hz, 2H).

^{13}C NMR (100 MHz, d_6-DMSO): 162.88, 162.83, 160.78, 153.94, 151.24, 149.83, 145.78, 139.94, 139.36, 131.29, 128.44, 127.86, 127.44, 124.46, 123.31, 113.48, 99.14.
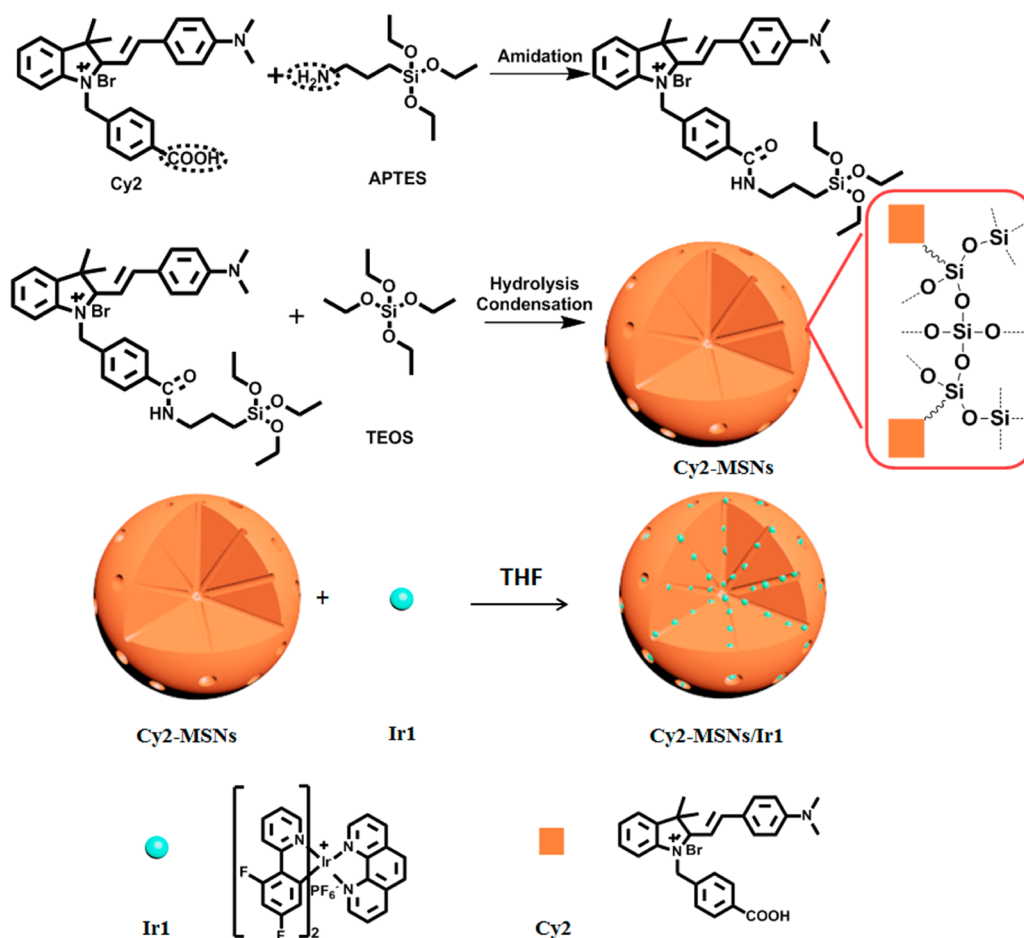
Figure 2. Synthetic procedure of **Cy2**-MSNs/**Ir1**, including the preparation of **Cy2**-MSNs using **Cy2**-binding silica precursors and TEOS, and adsorption process of **Ir1** onto the mesopores of **Cy2**-MSNs.

MS (ESI-MS): calcd. for $C_{34}H_{20}IrN_4PF_{10}$ 753.439 [M − PF$_6^-$ + H]$^+$.

Synthesis of Cy2. The merocyanine derivative **Cy2** was synthesized as follows. 1-(4-Carboxybenzyl)-2,3,3-trimethyl-3H-indol-1-ium (**L1**) bromide was prepared according to a reported procedure.[46] 2,3,3-Trimethylindolenine (11 mmol) and 4-(bromomethyl)benzoic acid (13 mmol) were dissolved in acetonitrile (20 mL). The solution was refluxed for overnight, and the resulting solid was collected by filtration. The solid was washed with acetonitrile and dried under reduced pressure to afford **L1** as a brown-pink solid. The 20 mL acetic acid solution containing **L1** (1.0 mmol) and 4-(dimethylamino)benzaldehyde (3.0 mmol) was refluxed at 50 °C with stirring for 12 h and then evaporated under reduced pressure. The resulting solid was suspended in solution containing 10 mL of MeOH, 10 mL of CH_2Cl_2 and 2 mL of petroleum ether. Finally, **Cy2** was collected by filtration (yield 78%).

^{1}H NMR (400 MHz, d_6-DMSO): δ (ppm) 8.42 (d, J = 14.4 Hz, 1H), 8.04 (d, J = 8.0 Hz, 2H), 7.95 (d, J = 8.0 Hz, 2H), 7.82−7.79 (m, 1H), 7.56−7.54 (m, 1H), 7.49−7.43 (m, 4H), 7.33 (d, J = 14.4 Hz, 1H), 6.88 (d, J = 9.6 Hz, 2H), 5.90 (s, 2H), 3.17 (s, 6H), 1.82 (s, 6H).

^{13}C NMR (100 MHz, d_6-DMSO): 180.01, 166.81, 155.57, 155.01, 142.42, 141.27, 139.31, 130.68, 130.07, 128.84, 128.82, 127.37, 126.85, 122.92, 122.44, 113.49, 112.47, 104.25, 50.94, 47.71, 39.98, 26.76.

MS (ESI-MS): calcd. for $C_{28}H_{29}BrN_2O_2$ 426.315 [M − Br$^-$ + H]$^+$.

Synthesis of Cy2-MSNs. The detailed preparation procedure of **Cy2**-MSNs contained three steps. First, the **Cy2**-binding silica precursor was performed as follows. (3-Aminopropyl)triethoxysilane (APTES) (2×10^{-5} mol) and **Cy2** (10^{-5} mol) were dissolved in 1 mL of N,N-dimethylformamide (DMF). 1-(3-(Dimethylamino)propyl)-3-ethylcarbodiimide hydrochloride (10^{-5} mol) and N-hydroxysuccinimide (2.5×10^{-5} mol) were added to this solution. The mixture was stirred for 24 h at room temperature to form **Cy2**-binding silica precursors. And then etyltrimethylammonium chloride (CTAC, 0.5 g, 1.56 mmol) was dissolved in 20 mL of deionized water, and the temperature of the mixture was adjusted to 95 °C. Subsequently, 0.40 mL of tetraethoxysilane (TEOS) and the above silica precursors were added to the surfactant solution under vigorous stirring. The mixture was then reacted for 6 h to give rise to a deep purple precipitate. The mixture was washed with ethanol for three times, and MSNs was dissolved in ethanol. Finally, the surfactant templates were removed by extraction in acidic ethanol.

Loading Ir1 into the Mesopores of Cy2-MSNs. Loading the iridium(III) complex **Ir1** into the mesopores of **Cy2**-MSNs was completed as follows. The surfactant-free MSNs materials were dispersed in 5 mL of THF solution, and the mixture was stirred with 3.8 mg of **Ir1** for 24 h. The as-prepared **Cy2**-MSNs/**Ir1** was washed by THF and collected by centrifugation at 11000 rpm for 10 min. Because the nanohybrid was prepared by mixing **Ir1** and **Cy2**-MSNs in the THF solution, the redundant **Ir1** that was not loaded into the mesopores was easily removed from the nanoparticles by washing with THF. The supernatant was collected and analyzed by UV/vis absorption spectrum. The absorption intensity of the extraction solution was used to compare with pure **Ir1** solutions with different concentrations.

H$_2$S Titration Experiments. Because the major form of H$_2$S exists as HS$^-$ in aqueous solution under the physiological pH of 7.4,[3] NaHS was used as a source of H$_2$S for titration experiments.

PLIM Imaging of Cy2-MSNs/Ir1 in PBS. PLIM imaging of **Cy2**-MSNs/**Ir1** at different concentrations of HS$^-$ were performed in PBS. First, the PBS solution containing 1 mg mL^{-1} **Cy2**-MSNs/**Ir1** and HS$^-$ with different concentrations (0, 192, 386, 600 μM) was obtained. And then 40 μL of solution was deposited on the slide. After
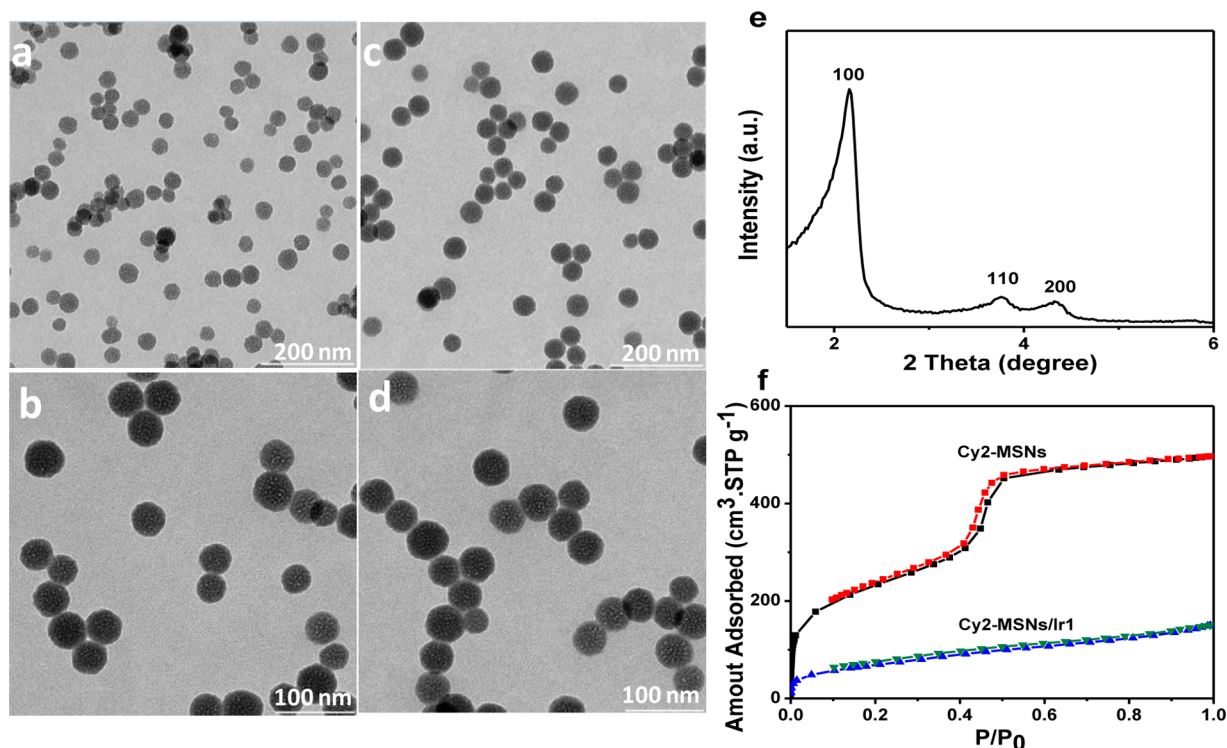
Figure 3. TEM images of (a,b) **Cy2**-MSNs and (c,d) **Cy2**-MSNs/**Ir1** dispersed in PBS (pH 7.4), (e) XRD patterns of **Cy2**-MSNs, $2\theta = 1.5-10°$, (f) nitrogen adsorption/desorption isotherms of **Cy2**-MSNs and **Cy2**-MSNs/**Ir1**.

the slide was positioned on the microscope objective, the PLIM images were obtained in a PLIM setup integrated with an Olympus IX81 laser scanning confocal microscope. The luminescence signal was detected by the system of the confocal microscope, and correlative calculation of the data was performed by professional software which was provided by PicoQuant Company. The light from the pulse diode laser head (PicoQuant, PDL 800-D) with an excitation wavelength of 405 nm and frequency of 0.5 MHz was focused onto the sample with a 40×/NA 0.95 objective lens for single-photon excitation.

Cell Culture and Cytotoxicity. The hepatocellular carcinoma cell line (HepG2 cells) was supplied by the Institute of Biochemistry and Cell Biology, SIBS, CAS (China). The cells were grown in RPMI 1640 (Roswell Park Memorial Institute's Medium) supplemented with 10% FBS at 37 °C and 5% CO_2. Cells (5×10^8/L) were placed on 18 mm glass coverslips and allowed to adhere for 24 h. The cell imaging experiments were carried out with an Olympus IX81 laser scanning confocal microscope and a 60× oilimmersion objective lens. A diode laser served as an excitation source at 405 nm for the live HepG2 cells that were incubated with **Cy2**-MSNs/**Ir1** (10 μg mL^{-1}) solely for 2 h at 37 °C, and emission was collected at 480−540 and 560−650 nm. The PLIM image setup is integrated with an Olympus IX81 laser scanning confocal microscope. The luminescence signal was detected by the system of the confocal microscope, and correlative calculation of the data was performed by professional software that was provided by PicoQuant Company. The light from the pulse diode laser head (PicoQuant, PDL 800-D) with excitation wavelength of 405 nm and frequency of 0.5 MHz was focused onto the sample with a 40×/NA 0.95 objective lens for single-photon excitation.

The cytotoxicity of **Cy2**-MSNs/**Ir1** toward the hepatocellular carcinoma cell line (HepG2 cells) was measured by the methyl thiazolyl tetrazolium (MTT) assay. Before incubation at 37 °C and 5% CO_2 atmosphere for 24 h, HepG2 cells in log phase were seeded into a 96-well cell-culture plate at 1×10^4/well. The **Cy2**-MSNs/**Ir1** (100 mL/well) at concentrations of 25, 50, 100, 200 and 400 μg mL^{-1} was added to the wells of the treatment group, and MTT containing 0.2% DMSO (100 mL/well) to the negative control group. The cells incubated at 37 °C and 5% CO_2 atmosphere for 24 h. 20 mL of MTT solution (5 mg mL^{-1}) was added to each well of the 96-well assay

plate, and the solution was incubated for another 3 h under the same condition. A Tecan Infinite M200 monochromator-based multifunction microplate reader was used for measuring the OD570 (absorbance value) of each well referenced at 690 nm. The following formula was used to calculate the viability of cell growth: viability (%) = [(mean of absorbance value of treatment group)/(mean absorbance value of control)] × 100%.

RESULTS AND DISCUSSION

Design Principle of the Nanohybrid for Sensing H_2S. Our design principle was based on the energy transfer from **Ir1** to **Cy2**. As shown in Figure S4 in the Supporting Information, there is a good overlap between the emission band of **Ir1** at 520 nm and the excitation spectrum of **Cy2**, satisfying the basic requirement for energy transfer. Moreover, fluorescent **Cy2** showed weak absorption bands below 450 nm, thus the direct excitation of **Cy2** in this region was avoided. These spectral characteristics were favorable for the effective energy transfer from **Ir1** to **Cy2** in the H_2S-sensitive probe **Cy2**-MSNs/**Ir1**. We predicted that upon excitation at 405 nm, the energy transfer from **Ir1** to **Cy2** occurred, and concomitantly, a decrease in the emission lifetime of **Ir1**, accompanied by a dramatic increase in the emission lifetime of **Cy2**, was also expected. Upon addition of H_2S, the sensitive nucleophilic addition reaction of HS$^-$ to **Cy2** led to the rapid quenching of its fluorescence, while the phosphorescence from **Ir1** was not influenced, allowing the ratiometric detection of H_2S. Additionally, the decrease of emission lifetime of **Cy2**-MSNs/**Ir1** upon addition of HS$^-$ enabled the lifetime-based detection.

Synthesis and Characterization of Cy2-MSNs/Ir1. Figure 2 shows the detailed synthetic procedure for the nanohybrid. The synthetic route involved covalent incorporation of **Cy2** into MSNs (**Cy2**-MSNs), and the loading of **Ir1** into the mesopores (**Cy2**-MSNs/**Ir1**). First, **Cy2**-binding silica
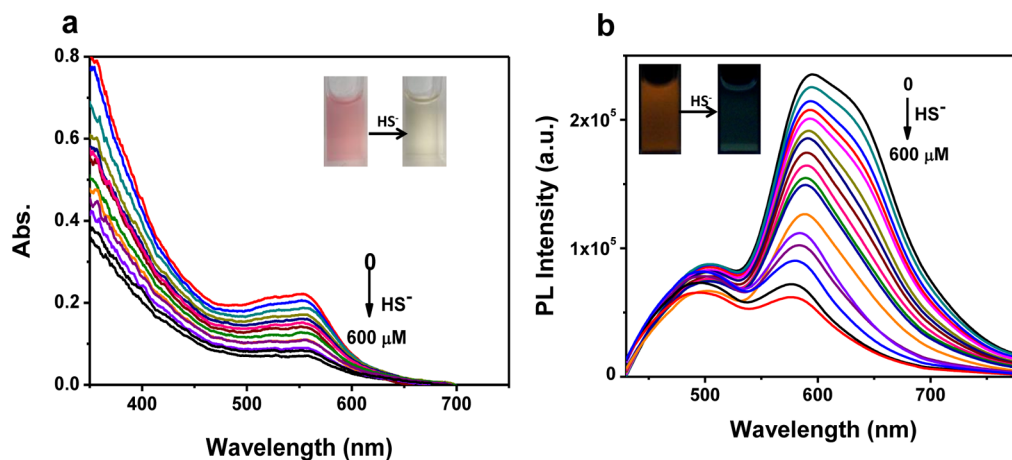
Figure 4. (a) Absorption spectra of **Cy2**-MSNs/**Ir1** (1 mg mL^{-1}) in PBS (pH = 7.4) obtained upon titration with HS$^-$ from 0 to 600 μM. (b) Photoluminescence spectra of **Cy2**-MSNs/**Ir1** (1 mg mL^{-1}) in PBS (pH = 7.4) obtained upon titration with HS$^-$ from 0 to 600 μM. λ_{ex} = 405 nm. Inset in panel a: photograph of 1 mg mL^{-1} **Cy2**-MSNs/**Ir1** in the absence or presence of HS$^-$. Inset in panel b: photograph of 1 mg mL^{-1} **Cy2**-MSNs/**Ir1** upon irradiation by a UV lamp (365 nm) in the absence or presence of HS$^-$.

precursors were formed through the amidation reaction between the amino group of (3-aminopropyl)triethoxysilane (APTES) and the carboxylic acid group of **Cy2**. And then **Cy2**-binding silica precursors and tetraethyl orthosilicate (TEOS) were added to the surfactant hexadecyl trimethylammonium chloride (CTAC) solution to hydrolyze and condense silicon alkoxides, yielding monodispersed mesoporous silica spheres containing **Cy2** (**Cy2**-MSNs). After removal of CTAC, positively charged **Ir1** was adsorbed onto the mesopores of **Cy2**-MSNs through electrostatic interaction between **Ir1** and the surface silanol groups (Figure S9 in the Supporting Information). Finally, the obtained nanohybrid **Cy2**-MSNs/**Ir1** was well dispersed in PBS.

Transmission electron microscopy (TEM) images showed that the monodispersed particle size of **Cy2**-MSNs was about 45 nm (Figure 3a,b), which was also in accord with the value obtained from HR-TEM and dynamic light scanning (DLS) (Figures S10a and S11a in the Supporting Information). Powder X-ray diffraction of **Cy2**-MSNs showed an intense peak (100) and two weak peaks (110, 200) (Figure 3e), which demonstrated the two-dimensional hexagonal symmetry. TEM, HR-TEM and DLS confirmed that there was no morphology change of MSNs after loading of **Ir1** (Figure 3c,d, and Figures S10b and S11b in the Supporting Information).

The physical properties of **Cy2**-MSNs and **Cy2**-MSNs/**Ir1** were analyzed by N$_2$ adsorption−desorption isotherms. **Cy2**-MSNs and **Cy2**-MSNs/**Ir1** exhibited type IV BET isotherms, which were typical for mesoporous materials. The H1-type hysteresis loop of **Cy2**-MSNs at partial pressure P/P_0 of 0.37−0.50 was observed, demonstrating the relatively uniform pore size distribution (Figure 3f). In contrast, the isotherms of **Cy2**-MSNs/**Ir1** showed a lower N$_2$ uptake, accounting for a decrease of specific surface area (from 838 m^2 g^{-1} to 252 m^2 g^{-1}, estimated by BET treatment of the isotherm). Additionally, the pore volume and pore size were obtained from the BJH method (Table S2 and Figure S12 in the Supporting Information). **Cy2**-MSNs showed a pore volume of 0.77 cm^3 g^{-1} and a narrow distribution of the pore size (3.67 nm). After **Ir1** was loaded into the mesopores, the pore volume decreased to 0.23 cm^3 g^{-1}. This change also confirmed the immobilization of **Ir1** on the internal pore of MSNs. Because the void space

inside the mesopores was occupied after immobilization of **Ir1**, the BJH pore size of **Cy2**-MSNs/**Ir1** decreased to 2.50 nm.

Photophysical Properties of Cy2-MSNs/Ir1. The UV/vis absorption spectrum of **Cy2**-MSNs/**Ir1** is shown in Figure S14a in the Supporting Information. The intense absorption band of fluorescent **Cy2** at 560 nm (ε/dm^3 mol^{-1} cm^{-1} 13 931) was assigned to the strong internal charge transfer (ICT) from N,N-dimethylaniline moiety to the indolenium moiety, which was demonstrated by theoretical calculation (Figure S5 and Table S1 in the Supporting Information). **Ir1** displayed the intense singlet metal-to-ligand charge-transfer state (^{1}MLCT) around 360 nm (ε/dm^3 mol^{-1} cm^{-1} 105 700). Weak absorption bands from a triplet metal-to-ligand charge-transfer state (^{3}MLCT) or ligand-centered charge-transfer state (^{3}LC) were also observed in the range of 400−500 nm in the absorption spectrum of **Ir1**. **Cy2**-MSNs displayed an intense absorption band at 568 nm, which indicated the covalent incorporation of **Cy2** into the siloxane network. The little red-shift of ICT band compared to fluorescent **Cy2** molecule was observed, and intense absorption from 300 to 450 nm was due to the scattering effect of MSNs. For **Cy2**-MSNs/**Ir1**, the bands at 360 and 565 nm also demonstrated that dye **Cy2** and complex **Ir1** were included in the nanohybrid. The loading amount of **Ir1** in the nanohybrid was determined to be 43.3 wt % through the subtraction method mentioned in the Experimental Section (Figure S15 in the Supporting Information).

In the PL spectra (Figure S14b in the Supporting Information), **Ir1** displayed a broad emission band at around 520 nm under excitation at 405 nm. Upon excitation at 540 nm, a major emission band at 596 nm was observed in the PL spectra of **Cy2** and **Cy2**-MSNs, indicating that the fluorescent property of **Cy2** was not affected by the covalent doping method into MSNs. **Cy2**-MSNs/**Ir1** displayed two broad emission bands with maxima at 500 and 596 nm, which were assigned to the luminescence emission of **Ir1** and **Cy2**, respectively. The nanohybrid exhibited two separated emission bands at 500 and 596 nm with little cross interference, which enabled the ratiometric detection. The luminescence quenching effect at 520−540 nm was mainly ascribed to the energy transfer from **Ir1** to **Cy2**. Moreover, **Cy2** was not excited at 405 nm according to the fluorescence spectrum illustrated in Figure S16 in the Supporting Information. The intense emission of
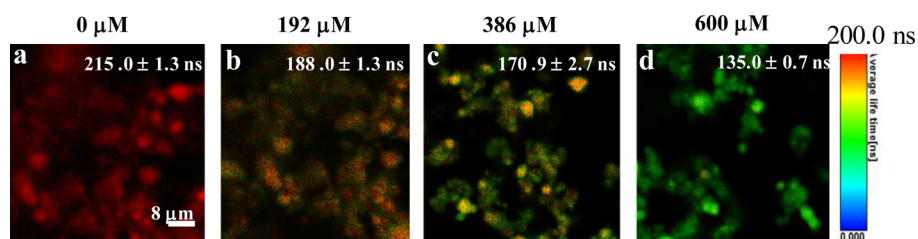
Figure 5. PLIM images (a−d) of 1 mg mL^{-1} **Cy2**-MSNs/**Ir1** in PBS (pH = 7.4) upon addition of different concentrations of HS$^-$.
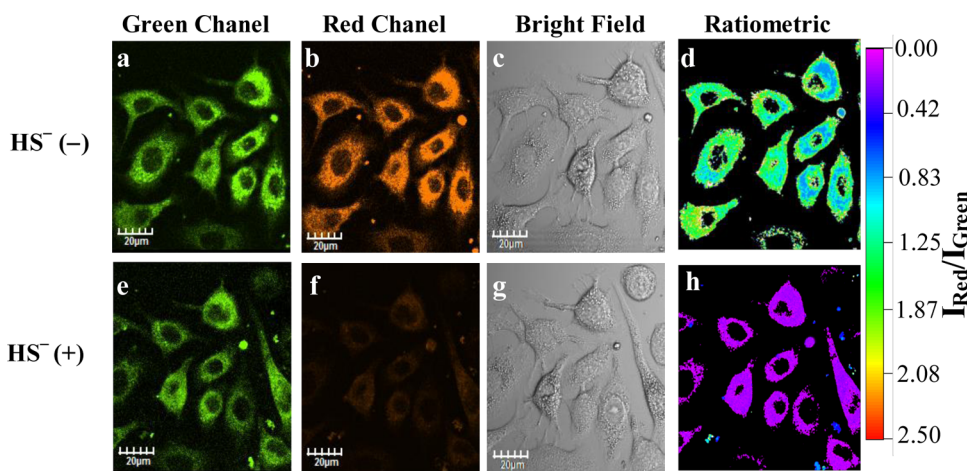

Figure 6. Ratiometric confocal luminescence images in live HepG2 cells constained by 10 μg mL^{-1} **Cy2**-MSNs/**Ir1** (a−d) and cells of pretreated with 10 μg mL^{-1} **Cy2**-MSNs/**Ir1** followed by incubation with HS$^-$ (600 μM) for 8 min (e−h). Emission was collected by green channel at 480−540 nm (a and e) and red channel at 560−650 nm (b and f), under excitation at 405 nm. (c and g) Bright-field images. (d and h) Ratiometric confocal fluorescence images with ratio of red to green channels.

Cy2 at 596 nm should be attributed to the efficient energy transfer, which was also confirmed by the observations that the emission lifetime of **Ir1** at 500 nm was shortened in **Cy2**-MSNs/**Ir1** (308 ns) than that of MSNs-loaded **Ir1** in PBS (984 ns), whereas **Cy2** displayed an extended emission lifetime at 596 nm in **Cy2**-MSNs/**Ir1** (105 ns). The energy transfer efficiency is determined to be 68.7% according to the following equation:[47]

$$E = 1 - \tau_{DA}/\tau_D$$

where τ_D is the lifetime of the donor in the absence of acceptor, and τ_{DA} is the lifetime of the donor in the presence of acceptor.

H$_2$S Detection of Cy2-MSNs/Ir1. The sensing performances of **Cy2**-MSNs/**Ir1** toward H$_2$S were studied in PBS. The **Cy2**-MSNs/**Ir1** solution (1 mg mL^{-1}) exhibited a dramatic decrease of the absorption peak at 565 nm in the presence of 600 μM of HS$^-$, leading to a color change of the solution from pink to yellow (Figure 4a). In the emission titration, addition of HS$^-$ selectively quenched the emission of **Cy2** at 596 nm, which was similar to the response of dye **Cy2** to HS$^-$ (Figure S6 in the Supporting Information) and ascribed to the rapid nucleophilic addition of HS$^-$ to the indolenium C-2 atom of **Cy2** (Figures S7 and S8 in the Supporting Information), while the emission intensity of **Ir1** at 500 nm remained unchanged (Figure 4b). A marked red-to-blue emission color change in response to H$_2$S was observed. Utilizing the ratio variation of emission intensity (I_{596}/I_{500}), a linear response to HS$^-$ was obtained over a wide concentration range (from 45.0 to 350.0 μM) (Figure S18 in the Supporting Information). The limit of detection (LOD) was determined to be as low as 2.7 μM,

which is lower than that of the endogenous H$_2$S concentration (10.0 to 600.0 μM) in the brain of bovine, rat and human.[6,48]

Meanwhile, upon addition of HS$^-$, the emission lifetime of **Cy2**-MSNs/**Ir1** showed a significant decrease at 596 nm from 105 to 70 ns, while the phosphorescence lifetime of **Ir1** at 500 nm did not change (307 ns). The luminescence lifetimes of **Cy2** in PBS (2% DMSO) solution before and after addition of HS$^-$ were also measured. The lifetimes were observed to change from 0.50 to 0.51 ns. Compared with the emission lifetime changes of **Cy2**, the lifetime changes of **Cy2**-MSNs/**Ir1** before and after addition of HS$^-$ were more sensitive. Additionally, the dynamic spatial distributions of the average luminescence lifetimes of **Cy2**-MSNs/**Ir1** were also visualized in PLIM imaging (Figure 5). The average luminescence lifetime of **Cy2**-MSNs/**Ir1** was measured to be 215.0 ns. Upon addition of NaHS, the lifetime was reduced from 215.0 ± 1.3 to 135.0 ± 0.7 ns, indicative of the possibility of PLIM for lifetime-based detection in biological samples.

The selectivity of **Cy2**-MSNs/**Ir1** to HS$^-$ was investigated in PBS (Figure S19 in the Supporting Information). In contrast to the dramatic response to HS$^-$ (300 μM), various biologically relevant anions (F$^-$, Cl$^-$, HCO$_3^-$, SCN$^-$, SO$_3^{2-}$, H$_2$O$_2$, ClO$^-$, NO$_3^-$, S$_2$O$_3^{2-}$, SO$_4^{2-}$, 6 mM) triggered negligible changes of the intensity ratio I_{596}/I_{500}. The ratiometric HS$^-$ sensing was also carried out in the presence of other biological thiols. Although excessive glutathione (GSH) and bovine serum albumin (BSA) showed minor interference to HS$^-$ sensing with respective quenching of 3% and 8% of the emission intensity, the selectivity of HS$^-$ sensing was not influenced. This phenomenon was attributed to the relative lower pK_a value (∼7.0) of H$_2$S, whereas the pK_a values of other biothiols

reached around 8.5,[49] thus making H$_2$S a better nucleophile than other biothiols in neutral medium. Additionally, the pH effects on **Cy2**-MSNs/**Ir1** were also investigated (Figure S20 in the Supporting Information). The emission intensity ratio I_{596}/I_{500} showed very minor change in the pH range from 4.0 to 9.0, thus demonstrating the stability of **Cy2**-MSNs/**Ir1**.

Application of Cy2-MSNs/Ir1 in Cellular Imaging. The cytotoxicity of **Cy2**-MSNs/**Ir1** toward the hepatocellular carcinoma cell line (HepG2 cells) was measured using the 3-(4,5-dimethylthiazol-2-yl)-2,5-diphenyltetrazolium bromide (MTT) assay to evaluate the potential application of **Cy2**-MSNs/**Ir1** in live cell imaging. The cellular viability was estimated to be greater than 82% after 24 h at the concentration of 400 μg mL^{-1} for **Cy2**-MSNs/**Ir1**, suggesting the low cytotoxicity of **Cy2**-MSNs/**Ir1** (Figure S21 in the Supporting Information). Practical applications of **Cy2**-MSNs/**Ir1** in imaging live HepG2 cells were investigated using confocal luminescence microscopy with a 405 nm Ar$^+$ laser. The confocal luminescence microscopy images are shown in Figure 6. After incubation of HepG2 cells with **Cy2**-MSNs/**Ir1** (10 μg mL^{-1}) for 2 h at 37 °C, intense luminescence was detected at green (480−540 nm) and red (560−650 nm) channels in the cytoplasm of the cells, demonstrating the good cell permeability of **Cy2**-MSNs/**Ir1**. Following supplement of 600 μM HS$^-$ in the growth media, a rapid and obvious quenching at the red channel over green channel was observed, suggesting the reaction of the nanohybrid to HS$^-$. Bright-field measurements indicated that the cells before and after treatment with HS$^-$ remained viable throughout the imaging experiments. Additionally, the ratiometric luminescence imaging was further investigated. The emission ratio at the red channel to the green channel decreased from 1.2 to 0.2 upon addition of HS$^-$ (Figure 6d,h).

Lifetime-based detection of H$_2$S was conducted in PLIM imaging. As shown in Figure 7a,b, cells treated with 10 μg mL^{-1}
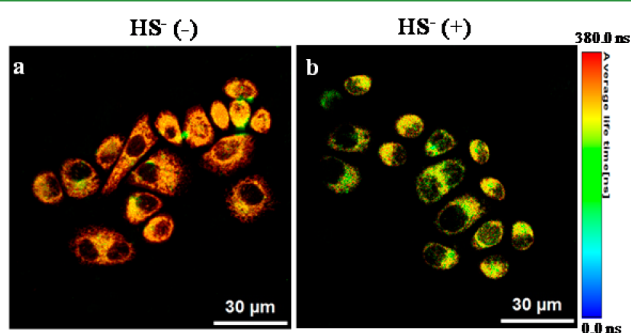

Figure 7. PLIM images in live HepG2 cells constained by 10 μg mL^{-1} **Cy2**-MSNs/**Ir1** (a) and cells pretreated with 10 μg mL^{-1} **Cy2**-MSNs/**Ir1** followed by incubation with HS$^-$ (600 μM) for 8 min (b).

Cy2-MSNs/**Ir1** for 2 h at 37 °C displayed a long luminescence lifetime of 414 ns. When 600 μM HS$^-$ was added in the growth media, the lifetime of microregions decreased to 366 ns, which was attributed to the quenching of the emission of the nanohybrid. Noticeably, because intracellular substrates provided a relatively enclosed environment to withstand oxygen invasion, the intracellular luminescence lifetime measured by PLIM was longer than that in aqueous solution. This result implied that **Cy2**-MSNs/**Ir1** was able to serve as a potential candidate for mapping HS$^-$ concentration in a complicated environment.

CONCLUSIONS

In summary, we have demonstrated a highly sensitive water-dispersible nanohybrid, **Cy2**-MSNs/**Ir1**, for the detection of H$_2$S. **Cy2**-MSNs/**Ir1** displayed two emission bands with maxima at 500 and 596 nm. Upon addition of NaHS, the emission at 596 nm was quenched, while the emission at 500 nm was almost unchanged. Using the emission intensity ratio at 596 nm over 500 nm as the detection signal, **Cy2**-MSNs/**Ir1** realized the selective and sensitive ratiometric detection of H$_2$S in aqueous solution with a detection limit of 2.7 μM. This detection limit was lower than the reported endogenous H$_2$S level in the brain of bovine, rat and human. Use of **Cy2**-MSNs/**Ir1** for ratiometric detection of intracellular H$_2$S was also demonstrated via confocal luminescence microscopy. Significantly, due to the efficient energy transfer from **Ir1** to **Cy2**, long-lived **Cy2**-MSNs/**Ir1** was applied for lifetime-based detection of H$_2$S via PLIM. As far as we know, this is the first example of lifetime-based imaging of H$_2$S in live cells. The probe opens up a novel strategy for lifetime-based detection of important analytes associated with biological processes.

ASSOCIATED CONTENT

Ⓢ Supporting Information
^{1}H NMR, ^{13}C NMR and MS results of **Cy2**; normalized PL spectra of **Cy2** and **Ir1**, and the normalized excitation spectrum of **Cy2**; theoretical calculation; additional characterization details of **Cy2**-MSNs and **Cy2**-MSNs/**Ir1**; titration experiments of **Cy2** and **Cy2**-MSNs; response of **Cy2** to HS$^-$ in ^{1}H NMR and MS spectra; selectivity, pH effects and cytotoxicity experiments of **Cy2**-MSNs/**Ir1**. This material is available free of charge via the Internet at http://pubs.acs.org.

AUTHOR INFORMATION

Corresponding Authors
*Qiang Zhao. E-mail: iamqzhao@njupt.edu.cn.
*Wei Huang. E-mail: wei-huang@njtech.edu.cn.
Notes
The authors declare no competing financial interest.

ACKNOWLEDGMENTS

REFERENCES

(1) Wang, R. Two's Company, Three's a Crowd: Can H$_2$S Be the Third Endogenous Gaseous Transmitter? *FASEB J.* **2002**, *16*, 1792−1798.
(2) Szabo, C.; Ransy, C.; Módis, K.; Andriamihaja, M.; Murghes, B.; Coletta, C.; Olah, G.; Yanagi, K.; Bouillaud, F. Regulation of Mitochondrial Bioenergetic Function By Hydrogen Sulfide. Part I. Biochemical and Physiological Mechanisms. *Br. J. Pharmacol.* **2014**, *171*, 2099−2122.
(3) Kabil, O.; Banerjee, R. Redox Biochemistry of Hydrogen Sulfide. *J. Biol. Chem.* **2010**, *285*, 21903−21907.
(4) Singh, S.; Padovani, D.; Leslie, R. A.; Chiku, T.; Banerjee, R. Relative Contributions of Cystathionine β-Cynthase and γ-Cystathio-

nase to H₂S Biogenesis via Alternative Trans-Sulfuration Reactions. *J. Biol. Chem.* **2009**, *284*, 22457−22466.

(5) Li, L.; Rose, P.; Moore, P. K. Hydrogen Sulfide and Cell Signaling. *Annu. Rev. Pharmacol. Toxicol.* **2011**, *51*, 169−187.

(6) Papapetropoulos, A.; Pyriochou, A.; Altaany, Z.; Yang, G.; Marazioti, A.; Zhou, Z.; Jeschke, M. G.; Branski, L. K.; Herndon, D. N.; Wang, R.; Szabó, C. Hydrogen Sulfide Is an Endogenous Stimulator of Angiogenesis. *Proc. Natl. Acad. Sci. U. S. A.* **2009**, *106*, 21972−21977.

(7) He, X.-L.; Yan, N.; Zhang, H.; Qi, Y.-W.; Zhu, L.-J.; Liu, M.-J.; Yan, Y. Hydrogen Sulfide Improves Spatial Memory Impairment and Decreases Production of Abeta in APP/PS1 Transgenic Mice. *Neurochem. Int.* **2014**, *67*, 1−8.

(8) Kamoun, P.; Belardinelli, M.-C.; Chabli, A.; Lallouchi, K.; Chadefaux-Vekemans, B. Endogenous Hydrogen Sulfide Overproduction in Down Syndrome. *Am. J. Med. Genet., Part A* **2003**, *116*, 310−311.

(9) Szabo, C. Roles of Hydrogen Sulfide in the Pathogenesis of Diabetes Mellitus and Its Complications. *Antioxid. Redox Signaling* **2012**, *17*, 68−80.

(10) Lippert, A. R.; New, E. J.; Chang, C. J. Reaction-based Fluorescent Probes for Selective Imaging of Hydrogen Sulfide in Living Cells. *J. Am. Chem. Soc.* **2011**, *133*, 10078−10080.

(11) Lin, V. S.; Lippert, A. R.; Chang, C. J. Cell-Trappable Fluorescent Probes for Endogenous Hydrogen Sulfide Signaling and Imaging H₂O₂-Dependent H₂S Production. *Proc. Natl. Acad. Sci. U. S. A.* **2013**, *110*, 7131−7135.

(12) Bae, S. K.; Heo, C. H.; Choi, D. J.; Sen, D.; Joe, E.-H.; Cho, B. R.; Kim, H. M. A Ratiometric Two-Photon Fluorescent Probe Reveals Reduction in Mitochondrial H₂S Production in a Parkinson's Disease Gene Knockout Astrocytes. *J. Am. Chem. Soc.* **2013**, *135*, 9915−9923.

(13) Yu, C.; Li, X.; Zeng, F.; Zheng, F.; Wu, S. Carbon-Dot-based Ratiometric Fluorescent Sensor for Detecting Hydrogen Sulfide in Aqueous Media and inside Live Cells. *Chem. Commun.* **2013**, *49*, 403−405.

(14) Qian, Y.; Karpus, J.; Kabil, O.; Zhang, S.-Y.; Zhu, H.-L.; Banerjee, R.; Zhao, J.; He, C. Selective Fluorescent Probes for Live-Cell Monitoring of Sulphide. *Nat. Commun.* **2011**, *2*, 495.

(15) Yu, F.; Li, P.; Song, P.; Wang, B.; Zhao, J.; Han, K. An ICT-based Strategy to a Colorimetric and Ratiometric Fluorescence Probe for Hydrogen Sulfide in Living Cells. *Chem. Commun.* **2012**, *48*, 2852−2854.

(16) Qian, Y.; Zhang, L.; Ding, S.; Deng, X.; He, C.; Zheng, X. E.; Zhu, H.-L.; Zhao, J. A Fluorescent Probe for Rapid Detection of Hydrogen Sulfide in Blood Plasma and Brain Tissues in Mice. *Chem. Sci.* **2012**, *3*, 2920−2923.

(17) Wang, X.; Sun, J.; Zhang, W.; Ma, X.; Lv, J.; Tang, B. A near-Infrared Ratiometric Fluorescent Probe for Rapid and Highly Sensitive Imaging of Endogenous Hydrogen Sulfide in Living Cells. *Chem. Sci.* **2013**, *4*, 2551−2556.

(18) Liu, C.; Pan, J.; Li, S.; Zhao, Y.; Wu, L. Y.; Berkman, C. E.; Whorton, A. R.; Xian, M. Capture and Visualization of Hydrogen Sulfide by a Fluorescent Probe. *Angew. Chem., Int. Ed.* **2011**, *50*, 10327−10329.

(19) Wang, J.; Lin, W.; Li, W. Three-Channel Fluorescent Sensing via Organic White Light-Emitting Dyes for Detection of Hydrogen Sulfide in Living Cells. *Biomaterials* **2013**, *34*, 7429−7436.

(20) Wang, B.; Li, Peng; Yu, F.; Song, P.; Sun, X.; Yang, S.; Lou, Z.; Han, K. A Reversible Fluorescence Probe Based on Se-BODIPY for the Redox Cycle between HClO Oxidative Stress and H₂S Repair in Living Cells. *Chem. Commun.* **2013**, *49*, 1014−1016.

(21) Lou, Z.; Li, P.; Han, K. Selenium as a Versatile Center in Fluorescence Probe for the Redox Cycle Between HClO Oxidative Stress and H₂S Repair. In *Advanced Protocols in Oxidative Stress III*; Armstrong, D., Ed.; Springer: New York, 2015; Vol. *1208*, pp 97−110.

(22) Sasakura, K.; Hanaoka, K.; Shibuya, N.; Mikami, Y.; Kimura, Y.; Komatsu, T.; Ueno, T.; Terai, T.; Kimura, H.; Nagano, T. Development of a Highly Selective Fluorescence Probe for Hydrogen Sulfide. *J. Am. Chem. Soc.* **2011**, *133*, 18003−18005.

(23) Chen, Y.; Zhu, C.; Yang, Z.; Chen, J.; He, Y.; Jiao, Y.; He, W.; Qiu, L.; Cen, J.; Guo, Z. A Ratiometric Fluorescent Probe for Rapid Detection of Hydrogen Sulfide in Mitochondria. *Angew. Chem., Int. Ed.* **2013**, *52*, 1688−1691.

(24) Grichine, A.; Haefele, A.; Pascal, S.; Duperray, A.; Michel, R.; Andraud, C.; Maury, O. Millisecond Lifetime Imaging with a Europium Complex Using a Commercial Confocal Microscope under One or Two-Photon Excitation. *Chem. Sci.* **2014**, *5*, 3475−3485.

(25) Baggaley, E.; Gill, M. R.; Green, N. H.; Turton, D.; Sazanovich, I. V.; Botchway, S. W.; Smythe, C.; Haycock, J. W.; Weinstein, J. A.; Thomas, J. A. Dinuclear Ruthenium(II) Complexes as Two-photon, Time-Resolved Emission Microscopy Probes for Cellular DNA. *Angew. Chem., Int. Ed.* **2014**, *53*, 3367−3371.

(26) Dmitriev, R. I.; Kondrashina, A. V.; Koren, K.; Klimant, I.; Zhdanov, A. V.; Pakan, J. M. P.; McDermott, K. W.; Papkovsky, D. B. Small Molecule Phosphorescent Probes for O₂ Imaging in 3D Tissue Models. *Biomater. Sci.* **2014**, *2*, 853−866.

(27) Zhang, K. Y.; Zhang, J.; Liu, Y.; Liu, S.; Zhang, P.; Zhao, Q.; Tang, Y.; Huang, W. Core−Shell Structured Phosphorescent Nanoparticles for Detection of Exogenous and Endogenous Hypochlorite in Live Cells via Ratiometric Imaging and Photoluminescence Lifetime Imaging Microscopy. *Chem. Sci.* **2015**, *6*, 301−307.

(28) Bastiaens, P. I. H.; Squire, A. Fluorescence Lifetime Imaging Microscopy: Spatial Resolution of Biochemical Processes in the Cell. *Trends Cell Biol.* **1999**, *9*, 48−52.

(29) Berezin, M. Y.; Achilefu, S. Fluorescence Lifetime Measurements and Biological Imaging. *Chem. Rev.* **2010**, *110*, 2641−2684.

(30) Chen, M.; Lei, Z.; Feng, W.; Li, C.; Wang, Q.-M.; Li, F. A Phosphorescent Silver(I)-Gold(I) Cluster Complex That Specifically Lights up the Nucleolus of Living Cells with FLIM Imaging. *Biomaterials* **2013**, *34*, 4284−4295.

(31) Liu, C.; Wang, X.; Zhou, Y.; Liu, Y. Timing and Operating Mode Design for Time-Gated Fluorescence Lifetime Imaging Microscopy. *Sci. World J.* **2013**, *2013*, 801901.

(32) Shi, H.; Sun, H.; Yang, H.; Liu, S.; Jenkins, G.; Feng, W.; Li, F.; Zhao, Q.; Liu, B.; Huang, W. Cationic Polyfluorenes with Phosphorescent Iridium(III) Complexes for Time-Resolved Luminescent Biosensing and Fluorescence Lifetime Imaging. *Adv. Funct. Mater.* **2013**, *23*, 3268−3276.

(33) Chen, M.; Wu, Y.; Liu, Y.; Yang, H.; Zhao, Q.; Li, F. A Phosphorescent Iridium(III) Solvent Complex for Multiplex Assays of Cell Death. *Biomaterials* **2014**, *35*, 8748−8755.

(34) Baggaley, E.; Weinstein, J. A.; Williams, J. A. G. Lighting the Way to See inside the Live Cell with Luminescent Transition Metal Complexes. *Coord. Chem. Rev.* **2012**, *256*, 1762−1785.

(35) Woo, H.; Cho, S.; Han, Y.; Chae, W.-S.; Ahn, D.-R.; You, Y.; Nam, W. Synthetic Control over Photoinduced Electron Transfer in Phosphorescence Zinc Sensors. *J. Am. Chem. Soc.* **2013**, *135*, 4771−4787.

(36) Zhao, Q.; Li, F.; Huang, C. Phosphorescent Chemosensors Based on Heavy-Metal Complexes. *Chem. Soc. Rev.* **2010**, *39*, 3007−3030.

(37) Zhao, Q.; Huang, C.; Li, F. Phosphorescent Heavy-Metal Complexes for Bioimaging. *Chem. Soc. Rev.* **2011**, *40*, 2508−2524.

(38) Lo, K. K.-W.; Choi, A. W.-T.; Law, W. H.-T. Applications of Luminescent Inorganic and Organometallic Transition Metal Complexes as Biomolecular and Cellular Probes. *Dalton Trans.* **2012**, *41*, 6021−6047.

(39) Ma, D. L.; He, H. Z.; Leung, K. H.; Chan, D. S. H.; Leung, C. H. Bioactive Luminescent Transition-Metal Complexes for Biomedical Applications. *Angew. Chem., Int. Ed.* **2013**, *52*, 7666−7682.

(40) Ma, D. L.; Chan, D. S.; Leung, C. H. Group 9 Organometallic Compounds for Therapeutic and Bioanalytical Applications. *Acc. Chem. Res.* **2014**, *47*, 3614−3631.

(41) Shi, C.; Sun, H.; Tang, X.; Lv, W.; Yan, H.; Zhao, Q.; Wang, J.; Huang, W. Variable Photophysical Properties of Phosphorescent Iridium(III) Complexes Triggered by *closo*- and *nido*-Carborane Substitution. *Angew. Chem., Int. Ed.* **2013**, *52*, 13434−13438.

(42) You, Y.; Han, Y.; Lee, Y.-M.; Park, S. Y.; Nam, W.; Lippard, S. J. Phosphorescent Sensor for Robust Quantification of Copper(II) Ion. *J. Am. Chem. Soc.* **2011**, *133*, 11488−11491.

(43) Xu, W.; Zhao, X.; Lv, W.; Yang, H.; Liu, S.; Liang, H.; Tu, Z.; Xu, H.; Qiao, W.; Zhao, Q.; Huang, W. Rational Design of Phosphorescent Chemodosimeter for Reaction-based One- and Two-Photon and Time-Resolved Luminescent Imaging of Biothiols in Living Cells. *Adv. Healthcare Mater.* **2014**, *3*, 658−669.

(44) Tamayo, A. B.; Alleyne, B. D.; Djurovich, P. I.; Lamansky, S.; Tsyba, I.; Ho, N. N.; Bau, R.; Thompson, M. E. Synthesis and Characterization of Facial and Meridional Tris-cyclometalated Iridium-(III) Complexes. *J. Am. Chem. Soc.* **2003**, *125*, 7377−7387.

(45) You, Y.; Lee, S.; Kim, T.; Ohkubo, K.; Chae, W.-S.; Fukuzumi, S.; Jhon, G.-J.; Nam, W.; Lippard, S. J. Phosphorescent Sensor for Biological Mobile Zinc. *J. Am. Chem. Soc.* **2011**, *133*, 18328−18342.

(46) Oushiki, D.; Kojima, H.; Terai, T.; Arita, M.; Hanaoka, K.; Urano, Y.; Nagano, T. Development and Application of a near-Infrared Fluorescence Probe for Oxidative Stress Based on Differential Reactivity of Linked Cyanine Dyes. *J. Am. Chem. Soc.* **2010**, *132*, 2795−2801.

(47) Kim, S.; Ohulchanskyy, T. Y.; Pudavar, H. E.; Pandey, R. K.; Prasad, P. N. Organically Modified Silica Nanoparticles Co-encapsulating Photosensitizing Drug and Aggregation-Enhanced Two-Photon Absorbing Fluorescent Dye Aggregates for Two-Photon Photodynamic Therapy. *J. Am. Chem. Soc.* **2007**, *129*, 2669−2675.

(48) Abe, K.; Kimura, H. The Possible Role of Hydrogen Sulfide as an Endogenous Neuromodulator. *J. Neurosci.* **1996**, *16*, 1066−1071.

(49) Lutolf, M. P.; Tirelli, N.; Cerritelli, S.; Cavalli, L.; Hubbell, J. A. Systematic Modulation of Michael-Type Reactivity of Thiols through the Use of Charged Amino Acids. *Bioconjugate Chem.* **2001**, *12*, 1051−1056.